Bulk Viscosity, Thermoacoustic Boundary Layers, and Adsorption near the Critical Point of Xenon

K. A. Gillis, I. I. Shinder, and M. R. Moldover

Process Measurements Division, National Institute of Standards and Technology, Gaithersburg, Maryland 20899-8360, USA

(Received 14 April 2006; published 8 September 2006)

We present an improved model for the dissipation and dispersion in an acoustic resonator filled with xenon near its critical temperature T_c. We test the model with acoustic measurements in stirred xenon that have a temperature resolution of $(T - T_c)/T_c \approx 7 \times 10^{-6}$. The model includes the frequency-dependent bulk viscosity calculated numerically from renormalization-group theory and it includes critical-point adsorption. Because the density of adsorbed xenon exceeds the critical density, the bulk viscosity's effect on surface dissipation is reduced, thereby improving the agreement between theory and experiment.

DOI: 10.1103/PhysRevLett.97.104502 PACS numbers: 51.40.+p, 51.10.+y, 64.60.Ht, 64.70.Fx

Acoustic resonators are used for the most accurate measurements of the thermophysical properties of gases because the spectrum of resonances can be accurately calculated and measured [1]. However, acoustic resonators are rarely used to study liquid-vapor critical phenomena for two reasons: (1) the usual theory of acoustic resonators does not fully account for the critical behavior of the thermophysical properties, and (2) at equilibrium, near-critical fluids stratify in Earth's gravity. Recently, we developed a theory of acoustic resonators appropriate for near-critical fluids, and we greatly reduced stratification by stirring the fluid [2]. Here, we compare the data to an improved model that includes the frequency-dependent bulk viscosity $\zeta(\omega)$, as calculated numerically from renormalization-group (RG) theory [3]. We find small inconsistencies between the data and the theory. We suggest that these inconsistencies result from critical adsorption [4] of xenon on the metal walls of the resonator. Because adsorbed xenon has a greater-than-critical density, it reduces the effects of the walls and improves the agreement between the acoustic model and the data.

As reported in Ref. [2], we measured the resonance frequencies f_n and quality factors Q_n of six acoustic modes spanning the temperature range $7 \times 10^{-6} < t \equiv (T - T_c)/T_c < 4 \times 10^{-2}$ and spanning a factor of 27 in frequency at each temperature. For our lowest frequency mode, the condition $\omega\tau = 1$ occurred 75 times closer to T_c than previous ultrasonic measurements [5]. ($\omega = 2\pi \times$ frequency and τ is the relaxation time for critical fluctuations [2,3].) Two nearly identical resonators were filled with xenon at the critical density. In one resonator, the xenon was surrounded by stainless-steel walls; in the other, the xenon was insulated from the steel walls by an 80-μm-thick layer of the polymer poly-monochloro-para-xylylene. The polymer layer reduced the thermal dissipation (denoted Q_λ^{-1}) within the thermoacoustic boundary layer by a factor of 8 at $t \approx 1 \times 10^{-3}$.

Each mode of the resonator is defined by a fixed wave number. Therefore the resonance frequency changes in proportion to a change in the speed of sound. As T_c was approached from above on the critical isochore, the frequencies decreased by a factor of 2.2 and the Q's decreased by as much as a factor of 140. The scaling variable $\omega\tau$ increased by a factor of 5×10^6 (see Fig. 1). As part of the data analysis, the frequencies f_n and Q_n above $t = 10^{-3}$ (where the effects of bulk viscosity are negligible) were used to fit scaling functions for the heat capacity C_V and the thermal conductivity λ_T using theoretical values for the critical exponents [2]. The results from our new analysis of the measured dissipation and dispersion over the entire range is shown in Figs. 1 and 2, respectively. Figures 1(b) and 2(b) show that, when critical adsorption is included, the model and the measurements agree with

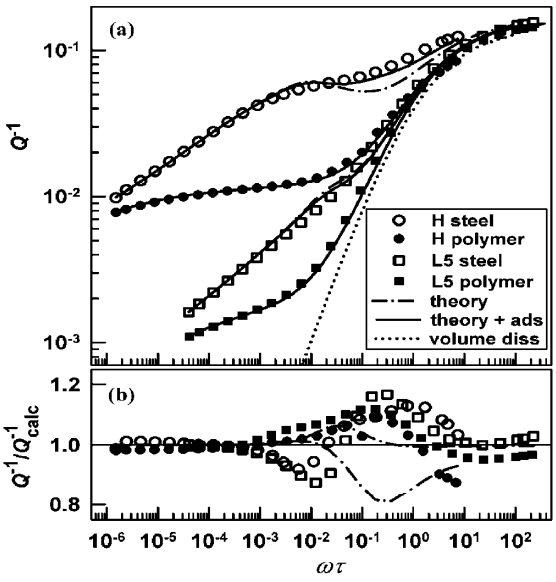

FIG. 1. (a) Points: quality factor data. Solid curves: present theory including critical adsorption. (The effect of critical adsorption was negligible for the polymer-coated resonator.) Dash-dotted curves: theory without adsorption. Dotted curve: volume dissipation only. (b) Ratio of the measured dissipation to the calculated dissipation including the effect of critical adsorption. Calculations use $v^* = 0.098$.

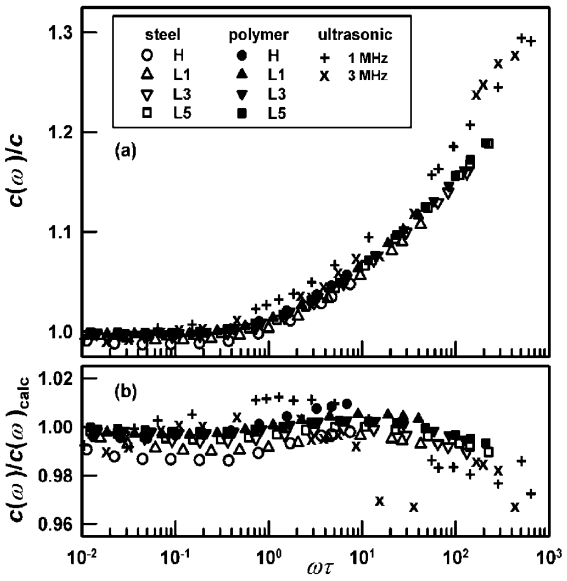

FIG. 2. (a) Ratio of the measured speed of sound at frequency ω to the calculated zero-frequency speed of sound. The resonance frequencies range from 0.12 to 7.5 kHz. Open symbols: steel resonator. Solid symbols: polymer-coated resonator. The ultrasonic data (×, +) are from 5. (b) Ratio of measured-to-calculated speed of sound using $\upsilon^* = 0.098$.

root-mean-squared deviations of 0.06 Q_n and 0.004 f_n, respectively. The numerically calculated values of $\zeta(\omega)$ are consistent with our low-frequency data (120 Hz to 7.5 kHz) and with the ultrasonic (0.4 MHz to 7 MHz) velocity data from Ref. [5]. However, the values of $\zeta(\omega)$ are not consistent with the ultrasonic attenuation data from Ref. [5]. When critical adsorption is ignored [dash-dotted line in Fig. 1(a)], the theory for the steel-walled cavity predicts a peak in the temperature dependence of Q_λ^{-1} (and the total dissipation Q^{-1}) for the lowest frequency mode (H) near $\omega\tau = 10^{-2}$ ($t = 2 \times 10^{-4}$) that we did not detect. Below, we estimate the effect of critical adsorption on the thermoacoustic boundary layer; the effect is large enough to suppress the predicted peak (solid lines in Fig. 1).

Figure 2 compares our measured frequency-dependent speed of sound and the theory. All of our data fall within $\pm 1.5\%$ of the theory. Remarkably, the data from the polymer-coated cavity fall within $\pm 0.35\%$ of a smooth function of $\omega\tau$. This illustrates the precision available from acoustic resonators.

Figure 2 also includes speed-of-sound data from the literature [5]. The speed-of-sound and attenuation data in Ref. [5] were acquired at ultrasonic frequencies without using resonators; therefore, they test $\zeta(\omega)$ without modeling the thermoacoustic boundary layers. Although the ultrasonic dispersion data in Fig. 2 is consistent with our calculation of $\zeta(\omega)$ with $\upsilon^* = 0.098$, the corresponding attenuation data is best described with $\upsilon^* = 0.063$, which is outside the predicted range. We do not have an explanation for this inconsistency.

We describe the resonator design and the experimental procedure briefly here; details are given in Ref. [2]. Each resonator was compact and had well-separated, low-frequency modes. The xenon-filled cavity consisted of two horizontal, cylindrical chambers that were connected by a reentrant cylindrical duct [2]. The lowest frequency resonance (120 Hz near T_c) is the Helmholtz mode (labeled "H") in which the xenon oscillates between the two cylindrical chambers through the duct. We also studied the first 5 longitudinal modes of the longer chamber (labeled "L1, ..., L5"). For these six modes, we accurately determined the wave numbers ($k_{a,n} \approx 12.26\ \mathrm{m}^{-1}, \ldots, 327.2\ \mathrm{m}^{-1}$) and the characteristic lengths for thermal $q_{T,n}$ and viscous $q_{v,n}$ dissipation by calibration with argon and from dimensions.

In thermal equilibrium near T_c, the xenon's density stratifies because of Earth's gravity. Following Cannell [6], we heated the bottom of each resonator. The resulting temperature gradient forced convection that stirred the xenon and replaced the isothermal density profile with a more uniform, nearly adiabatic density profile. The stirring also reduced the apparent equilibration time from several hours to approximately 1 min [2]. Because the cavity had cylindrical cross sections 16 and 23.5 mm high, the adiabatic gradient limited the effective temperature resolution of the stirred measurements to $t \approx 7 \times 10^{-6}$. Significantly, the measured frequencies and Q's were unchanged when the heater power stirring the xenon was increased eightfold.

The acoustic pressure was 100 Pa at $t = 3 \times 10^{-4}$ and 5 Pa at $t = 10^{-5}$. (For comparison, the pressure at the bottom of the cavity exceeds the pressure at the top by 200 Pa.) The resonance frequencies and Q's did not change when the acoustic drive level was increased 100-fold. Furthermore, we were unable to detect harmonics of the drive frequency; thus, we are confident that nonlinear acoustic phenomena are negligible.

The theory of the resonant cavity (neglecting adsorption) was described previously in detail [2]. It is based on the equations of linearized viscid hydrodynamics and heat transfer [2,7]. These equations have one propagating solution (the acoustic wave) and two evanescent solutions (thermal and shear waves). Allowing for the frequency-dependent bulk viscosity $\zeta(\omega)$ and for an arbitrarily large specific-heat ratio $\gamma \equiv C_P/C_V$, the exact dispersion relation for the propagating wave is

$$k_a^2 = (\omega^2/c^2) q_-^2(\omega),$$

with the definitions

$$q_-^2(\omega) \equiv 2(1 + i\Delta_v + i\gamma\Delta_T + \Xi)^{-1},$$

$$\Xi^2 \equiv (1 + i\Delta_v - i\gamma\Delta_T)^2 + 4i\Delta_T(\gamma - 1),$$

$$\Delta_v \equiv (\omega/\rho c^2)[\zeta(\omega) + (4/3)\eta], \qquad \Delta_T \equiv \omega D_T/c^2.$$

Here, $D_T \equiv \lambda_T/(\rho C_P)$ is the thermal diffusivity and η is the shear viscosity. We did account for the evanescent

viscous wave; however, we do not discuss it here because it has a minor effect in the present measurements despite the shear viscosity's weak divergence at the critical point [8]. The exact dispersion relation for the thermal wave is

$$k_T^2 = (\omega/2D_T)(1-i)^2/[(1+i\gamma\Delta_v)q_-^2(\omega)].$$

The boundary conditions at the walls are (1) rigid wall, (2) no slip, (3) continuous temperature (local equilibrium), and (4) energy conservation (continuous heat flow).

We satisfy the boundary conditions with a superposition of the three hydrodynamic waves and an evanescent temperature wave within the wall. The solution leads to equations for the resonance frequencies and Q's in terms of the thermophysical properties and the characteristic lengths $q_{T,n}$ and $q_{v,n}$ for the modes. These expressions are

$$f_n = \frac{c}{2\pi}\,\mathrm{Re}[k_{a,n}/q_-] \quad \text{and} \quad Q_n^{-1} = \frac{2\mathrm{Im}[k_{a,n}/q_-]}{\mathrm{Re}[k_{a,n}/q_-]}.$$

Far from T_c, the inverse quality factor Q^{-1} is the sum of three terms: viscous losses Q_η^{-1} and thermal losses Q_λ^{-1} within the thermoacoustic boundary layer and bulk losses Q_ζ^{-1} throughout the volume of the cavity. These terms are

$$\begin{aligned} Q_\eta^{-1} &\approx q_v\delta_v, \\ Q_\zeta^{-1} &\approx \omega\mathrm{Re}[\zeta]/(\rho c^2), \\ Q_\lambda^{-1} &\approx (\gamma-1)q_T\delta_T/[1+(\varepsilon_{\mathrm{xenon}}/\varepsilon_{\mathrm{wall}})], \\ \text{and} \quad \delta_T &\equiv (1-i)/k_T = (2D_T/\omega)^{1/2}(1+i\gamma\Delta_v)^{1/2}q_-. \end{aligned} \tag{1}$$

[$\varepsilon \equiv (\rho C_P \lambda_T)^{1/2}$ is the effusivity. For steel, we took $\varepsilon_{\mathrm{wall}}$ from the literature; for the polymer, we fitted $\varepsilon_{\mathrm{wall}}$ to the data far from T_c.] We emphasize that the approximations leading to Eq. (1) were not used in our analysis. If we consider only volume losses, i.e., we neglect the thermal and viscous boundary layers, then the dissipation would be given by the dotted curve in Fig. 1.

If the calculated properties of the thermoacoustic boundary layer were fully realized, they would be remarkable. The characteristic decay length is $\mathrm{Re}[\delta_T]$. As T_c is approached from above, this length decreases, reaching a minimum of 500 nm for the H mode at $t \approx 3\times10^{-4}$. Closer to T_c, $\mathrm{Re}[\delta_T]$ increases rapidly. Near the minimum, the nearly isothermal xenon in the boundary layer is so compressible that its acoustic admittance reduces the frequency of the H mode by 2%. For all the modes that we used, $\mathrm{Re}[\delta_T] > 10\xi$, justifying our use of local hydrodynamics. (ξ is the correlation length.)

The complete expressions for the thermophysical properties of xenon that we used in the theory are given in [2]. With auxiliary data from the literature, our data determine $C_V(t)$ with an uncertainty of 0.4%. (All uncertainties are standard uncertainties.) The results may be represented by

$$T_c\rho_c C_V/P_c \equiv C_V^* = A^+ t^{-\alpha}(1+C^+t^\Delta) + B^+,$$

with $A^+ = 18.01 \pm 0.11$, $B^+ = -18.04 \pm 0.27$, and $C^+ = 0.42 \pm 0.10$, assuming the theoretical values $\alpha = 0.110$ and $\Delta = 0.5$. We determined the relaxation time $\tau \equiv 6\pi\xi^3\eta/(k_B T_c)$ using the viscosity from the literature [8] and the correlation length amplitude $\xi_0^+ = (0.1866 \pm 0.0010)$ nm, obtained from A^+ and the theoretical amplitude ratio [2].

In the range $10^{-3} < t < 10^{-1}$, we fit the acoustic data to determine $\lambda_T(t)$ [2]. Closer to T_c, in the range $10^{-5} < t < 10^{-3}$, the Q's are sensitive to $\zeta(\omega)$. Previously [2], we assumed an *ad hoc* complex-valued expression for $\zeta(\omega)$ that had the expected limiting behavior for large and small values of $\omega\tau$. We noted then that the deviations between the theory and the data were sensitive to the interpolating function used for $\zeta(\omega)$. Here, we eliminate the problems with approximate analytic expressions. We numerically calculated $\zeta(\omega)$ from the RG expressions [3]

$$\begin{aligned} \zeta(\omega) &= v^*\rho c^2\tau(1+q_B)I(\omega\tau, q_B), \\ q_B &= -1 + C_V^*/(A^+t^{-\alpha}), \\ \text{and} \quad I(\omega\tau, q_B) &= \int_0^{\xi/a} \frac{x^2(1+q_B x^{\alpha/\nu})^{-2}dx}{(1+x^2)^{(1-\alpha)/\nu}[K'(x) + \frac{1}{2}i\omega\tau]}, \end{aligned} \tag{2}$$

where $K'(x) = (3/4)[1 + x^2 + (x^z - x^{-1})\tan^{-1}(x)]$ is the

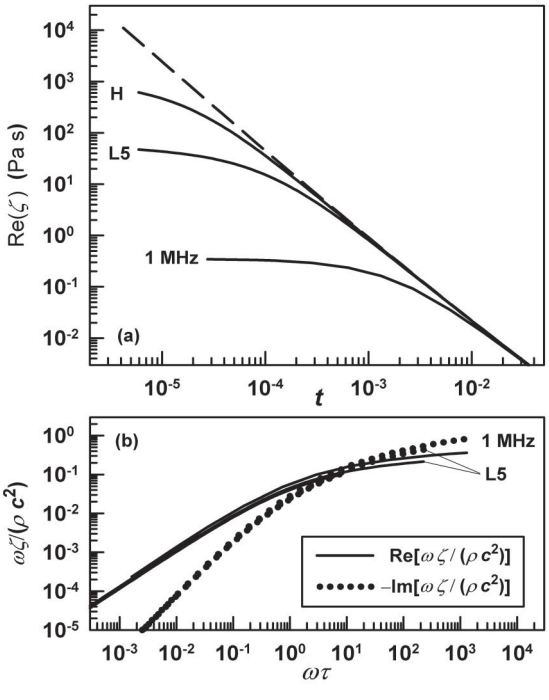

FIG. 3. The bulk viscosity of xenon in the critical region calculated numerically from Eq. (2) (with $v^* = 0.098$) for constant wave numbers 12.26 m^{-1} (H) and 327.2 m^{-1} (L5), constant frequency (1 MHz), and zero frequency (dashed line). (a) The real part as a function of reduced temperature t. (b) The real and imaginary parts of the (approximately) scaled form $\omega\zeta/(\rho c^2)$ as a function of the scaling variable $\omega\tau$.

Kawasaki function and $z = 3.0690 \pm 0.0006$ is the dynamic scaling exponent [8]. In Eq. (2), $x = k\xi$ is the dimensionless wave number that characterizes critical fluctuations. The upper limit corresponds to the inverse of the interparticle spacing a, and it cuts off the unphysical singularity at $|q_B|^{-\nu/\alpha}$ when $q_B < 0$. The constant v^* is predicted [3] to be between $\alpha/(2\nu) = 0.087$ (from expansion) and $2\alpha/(\nu z) = 0.114$ (from mode-coupling theory). We numerically calculated $\zeta(\omega)$ from Eq. (2) with $v^* = 0.098$ and the properties of xenon discussed above. Figure 3(a) shows the real part of $\zeta(\omega)$ as a function of t for constant wave numbers corresponding to the H and L5 modes, for constant frequency of 1 MHz, and for zero frequency. Figure 3(b) shows that both the real and imaginary parts of $\omega\zeta(\omega)/\rho c^2$ approximately scale with $\omega\tau$.

The theory of the resonator combined with our representations of the thermophysical properties explain the low-frequency data within $\pm 1.5\%$ of $c(\omega)$. However, the same theory predicts peaks in the temperature dependence of Q_λ^{-1} (at $t \approx 2 \times 10^{-4}$ for the H mode of the steel resonator) that we did not detect. This prediction occurs because, as T_c is approached from above, Q_λ^{-1} first increases with the diverging product $\gamma D_T^{1/2}$ until the effusivity of the xenon equals the effusivity of the wall. ($\varepsilon_{\text{xenon}} = \varepsilon_{\text{steel}}$ at $t \approx 6 \times 10^{-4}$.) At still smaller values of t, Q_λ^{-1} decreases because the strongly diverging bulk viscosity acting within the thermal boundary layer becomes important. Then, the bulk viscosity reduces the effective compressibility of the boundary layer and the dissipation within it.

We now consider the possibility that critical adsorption suppressed the peak in Q_λ^{-1}. We approximated the dispersion force acting between the steel wall and the xenon by the potential

$$V(y) \approx -(5 \times 10^{-49}\ \mathrm{J\,m^3})/y^3. \tag{3}$$

In Eq. (3), y measures the distance from the wall into the xenon, and the coefficient is typical for a metal-xenon interaction [9]. In equilibrium, the dispersion force's contribution to the chemical potential of xenon is balanced by an increase in the density of the xenon near the wall; i.e., xenon is adsorbed on the wall. We used Eq. (3) and the restricted cubic model equation of state [10] to calculate numerically the density profile $\rho(y, t)$. The results were consistent with the expectation that the thickness of the adsorbed layer is on the order of the correlation length. Thus, the adsorbed layer is much thinner than the thermoacoustic boundary layer [2,4].

From the adsorption profile $\rho(y, t)$, we estimated the other thermophysical properties of the adsorbed xenon. Because the adsorbed xenon is farther from the critical point than the bulk of the xenon, the adsorbed layer is less compressible and has a smaller effusivity. In effect, the adsorbed layer insulates the thermoacoustic boundary layer from the metal. Adsorption has a negligible effect in the polymer-coated cavity because the polymer's low effusivity already insulates the xenon from the underlying wall.

We estimated the layer's effects on the acoustic modes by replacing it with an isotropic slab with properties equal to their values averaged over y. The slab has a negligible effect on the resonance frequencies; however, it eliminates the peak in Q_λ^{-1}, as shown by the solid curves in Fig. 1. The systematic deviations in Fig. 1(b) occur when the bulk viscosity becomes important in the boundary layer [2]. Thus, a more rigorous model of critical adsorption may further improve the agreement with the data.

We thank Jim Mehl, Mikhail Anisimov, Greg Zimmerli, and Bobby Berg for advice and continuing interest. This research was supported, in part, by NASA Contract No. C-32088-K.

[1] M. R. Moldover, J. P. M. Trusler, T. J. Edwards, J. B. Mehl, and R. S. Davis, Phys. Rev. Lett. **60**, 249 (1988).
[2] K. A. Gillis, I. I. Shinder, and M. R. Moldover, Phys. Rev. E **70**, 021201 (2004); **72**, 051201 (2005).
[3] A. Onuki, Phys. Rev. E **55**, 403 (1997); A. Onuki, *Phase Transition Dynamics* (Cambridge University Press, Cambridge, 2002), Chap. 6.
[4] A. J. Liu and M. E. Fisher, Phys. Rev. A **40**, 7202 (1989); S. Dietrich and M. Napiórkowski, Phys. Rev. A **43**, 1861 (1991); G. Flöter and S. Dietrich, Z. Phys. B **97**, 213 (1995).
[5] P. E. Mueller, D. Eden, C. W. Garland, and R. C. Williamson, Phys. Rev. A **6**, 2272 (1972); the tabulated attenuation data were increased by 15% of α_λ as recommended in J. Thoen and C. W. Garland, Phys. Rev. A **10**, 1311 (1974).
[6] D. S. Cannell, Phys. Rev. A **12**, 225 (1975).
[7] P. M. Morse and K. U. Ingard, *Theoretical Acoustics* (McGraw-Hill, New York, 1968), Chap. 6.
[8] R. F. Berg, M. R. Moldover, and G. A. Zimmerli, Phys. Rev. E **60**, 4079 (1999); Phys. Rev. Lett. **82**, 920 (1999).
[9] G. Vidali, G. Ihm, H.-Y. Kim, and M. W. Cole, Surf. Sci. Rep. **12**, 135 (1991).
[10] M. R. Moldover, J. V. Sengers, R. W. Gammon, and R. J. Hocken, Rev. Mod. Phys. **51**, 79 (1979).